

# Experimental study of the atmospheric neutrino backgrounds for $p \rightarrow e^+ \pi^0$ searches in water Cherenkov detectors

S. Mine,<sup>4</sup> J. L. Alcaraz,<sup>1</sup> S. Andringa,<sup>1</sup> S. Aoki,<sup>14</sup> J. Argyriades,<sup>5</sup> K. Asakura,<sup>14</sup> R. Ashie,<sup>29</sup> F. Berghaus,<sup>3</sup> H. Berns,<sup>33</sup> H. Bhang,<sup>24</sup> A. Blondel,<sup>9</sup> S. Borghi,<sup>9</sup> J. Bouchez,<sup>5</sup> J. Burguet-Castell,<sup>32</sup> D. Casper,<sup>4</sup> J. Catala,<sup>32</sup> C. Cavata,<sup>5</sup> A. Cervera,<sup>9</sup> S. M. Chen,<sup>31</sup> K. O. Cho,<sup>6</sup> J. H. Choi,<sup>6</sup> U. Dore,<sup>23</sup> X. Espinal,<sup>1</sup> M. Fechner,<sup>5</sup> E. Fernandez,<sup>1</sup> Y. Fujii,<sup>11</sup> Y. Fukuda,<sup>19</sup> J. Gomez-Cadenas,<sup>32</sup> R. Gran,<sup>33</sup> T. Hara,<sup>14</sup> M. Hasegawa,<sup>16</sup> T. Hasegawa,<sup>11</sup> Y. Hayato,<sup>29</sup> R. L. Helmer,<sup>31</sup> K. Hiraide,<sup>16</sup> J. Hosaka,<sup>29</sup> A. K. Ichikawa,<sup>16</sup> M. Iinuma,<sup>12</sup> A. Ikeda,<sup>21</sup> T. Ishida,<sup>11</sup> K. Ishihara,<sup>29</sup> T. Ishii,<sup>11</sup> M. Ishitsuka,<sup>30</sup> Y. Itow,<sup>29</sup> T. Iwashita,<sup>11</sup> H. I. Jang,<sup>6</sup> E. J. Jeon,<sup>24</sup> I. S. Jeong,<sup>6</sup> K. K. Joo,<sup>24</sup> G. Jover,<sup>1</sup> C. K. Jung,<sup>27</sup> T. Kajita,<sup>30</sup> J. Kameda,<sup>29</sup> K. Kaneyuki,<sup>30</sup> I. Kato,<sup>31</sup> E. Kearns,<sup>2</sup> C. O. Kim,<sup>15</sup> M. Khabibullin,<sup>13</sup> A. Khotjantsev,<sup>13</sup> D. Kielczewska,<sup>34,25</sup> J. Y. Kim,<sup>6</sup> S. B. Kim,<sup>24</sup> P. Kitching,<sup>31</sup> K. Kobayashi,<sup>27</sup> T. Kobayashi,<sup>11</sup> A. Konaka,<sup>31</sup> Y. Koshio,<sup>29</sup> W. Kropp,<sup>4</sup> Yu. Kudenko,<sup>13</sup> Y. Kuno,<sup>22</sup> Y. Kurimoto,<sup>16</sup> T. Kutter,<sup>17,3</sup> J. Learned,<sup>10</sup> S. Likhoded,<sup>2</sup> I. T. Lim,<sup>6</sup> P. F. Loverre,<sup>23</sup> L. Ludovici,<sup>23</sup> H. Maesaka,<sup>16</sup> J. Mallet,<sup>5</sup> C. Mariani,<sup>23</sup> S. Matsuno,<sup>10</sup> V. Matveev,<sup>13</sup> K. McConnel,<sup>18</sup> C. McGrew,<sup>27</sup> S. Mikheyev,<sup>13</sup> A. Minamino,<sup>29</sup> O. Mineev,<sup>13</sup> C. Mitsuda,<sup>29</sup> M. Miura,<sup>29</sup> Y. Moriguchi,<sup>14</sup> S. Moriyama,<sup>29</sup> T. Nakadaira,<sup>11</sup> M. Nakahata,<sup>29</sup> K. Nakamura,<sup>11</sup> I. Nakano,<sup>21</sup> T. Nakaya,<sup>16</sup> S. Nakayama,<sup>30</sup> T. Namba,<sup>29</sup> R. Nambu,<sup>29</sup> S. Nawang,<sup>12</sup> K. Nishikawa,<sup>11</sup> K. Nitta,<sup>16</sup> F. Nova,<sup>1</sup> P. Novella,<sup>32</sup> Y. Obayashi,<sup>29</sup> A. Okada,<sup>30</sup> K. Okumura,<sup>30</sup> S. M. Oser,<sup>3</sup> Y. Oyama,<sup>11</sup> M. Y. Pac,<sup>7</sup> F. Pierre,<sup>5</sup> A. Rodriguez,<sup>1</sup> C. Saji,<sup>30</sup> M. Sakuda,<sup>21</sup> F. Sanchez,<sup>1</sup> K. Scholberg,<sup>8,18</sup> R. Schroeter,<sup>9</sup> M. Sekiguchi,<sup>14</sup> M. Shiozawa,<sup>29</sup> K. Shiraishi,<sup>33</sup> G. Sitjes,<sup>32</sup> M. Smy,<sup>4</sup> H. Sobel,<sup>4</sup> M. Sorel,<sup>32</sup> J. Stone,<sup>2</sup> L. Sulak,<sup>2</sup> A. Suzuki,<sup>14</sup> Y. Suzuki,<sup>29</sup> M. Tada,<sup>11</sup> T. Takahashi,<sup>12</sup> Y. Takenaga,<sup>30</sup> Y. Takeuchi,<sup>29</sup> K. Taki,<sup>29</sup> Y. Takubo,<sup>22</sup> N. Tamura,<sup>20</sup> M. Tanaka,<sup>11</sup> R. Terri,<sup>27</sup> S. T'Jampens,<sup>5</sup> A. Tornero-Lopez,<sup>32</sup> Y. Totsuka,<sup>11</sup> M. Vagins,<sup>4</sup> L. Whitehead,<sup>27</sup> C.W. Walter,<sup>8</sup> W. Wang,<sup>2</sup> R.J. Wilkes,<sup>33</sup> S. Yamada,<sup>29</sup> Y. Yamada,<sup>11</sup> S. Yamamoto,<sup>16</sup> C. Yanagisawa,<sup>27</sup> N. Yershov,<sup>13</sup> H. Yokoyama,<sup>28</sup> M. Yokoyama,<sup>16</sup> J. Yoo,<sup>24</sup> M. Yoshida,<sup>22</sup> and J. Zalipska<sup>25</sup>

(The K2K Collaboration)

<sup>1</sup>*Institut de Fisica d'Altes Energies, Universitat Autònoma de Barcelona, E-08193 Bellaterra (Barcelona), Spain*

<sup>2</sup>*Department of Physics, Boston University, Boston, Massachusetts 02215, USA*

<sup>3</sup>*Department of Physics & Astronomy, University of British Columbia, Vancouver, British Columbia V6T 1Z1, Canada*

<sup>4</sup>*Department of Physics and Astronomy, University of California, Irvine, Irvine, California 92697-4575, USA*

<sup>5</sup>*DAPNIA, CEA Saclay, 91191 Gif-sur-Yvette Cedex, France*

<sup>6</sup>*Department of Physics, Chonnam National University, Kwangju 500-757, Korea*

<sup>7</sup>*Department of Physics, Dongshin University, Naju 520-714, Korea*

<sup>8</sup>*Department of Physics, Duke University, Durham, North Carolina 27708, USA*

<sup>9</sup>*DPNC, Section de Physique, University of Geneva, CH1211, Geneva 4, Switzerland*

<sup>10</sup>*Department of Physics and Astronomy, University of Hawaii, Honolulu, Hawaii 96822, USA*

<sup>11</sup>*High Energy Accelerator Research Organization(KEK), Tsukuba, Ibaraki 305-0801, Japan*

<sup>12</sup>*Graduate School of Advanced Sciences of Matter, Hiroshima University, Higashi-Hiroshima, Hiroshima 739-8530, Japan*

<sup>13</sup>*Institute for Nuclear Research, Moscow 117312, Russia*

<sup>14</sup>*Kobe University, Kobe, Hyogo 657-8501, Japan*

<sup>15</sup>*Department of Physics, Korea University, Seoul 136-701, Korea*

<sup>16</sup>*Department of Physics, Kyoto University, Kyoto 606-8502, Japan*

<sup>17</sup>*Department of Physics and Astronomy, Louisiana State University, Baton Rouge, Louisiana 70803-4001, USA*

<sup>18</sup>*Department of Physics, Massachusetts Institute of Technology, Cambridge, Massachusetts 02139, USA*

<sup>19</sup>*Department of Physics, Miyagi University of Education, Sendai 980-0845, Japan*

<sup>20</sup>*Department of Physics, Niigata University, Niigata, Niigata 950-2181, Japan*

<sup>21</sup>*Department of Physics, Okayama University, Okayama, Okayama 700-8530, Japan*

<sup>22</sup>*Department of Physics, Osaka University, Toyonaka, Osaka 560-0043, Japan*

<sup>23</sup>*University of Rome La Sapienza and INFN, I-000185 Rome, Italy*

<sup>24</sup>*Department of Physics, Seoul National University, Seoul 151-747, Korea*

<sup>25</sup>*A. Soltan Institute for Nuclear Studies, 00-681 Warsaw, Poland*

<sup>26</sup>*Research Center for Neutrino Science, Tohoku University, Sendai, Miyagi 980-8578, Japan*

<sup>27</sup>*Department of Physics and Astronomy, State University of New York, Stony Brook, New York 11794-3800, USA*

<sup>28</sup>*Department of Physics, Tokyo University of Science, Noda, Chiba 278-0022, Japan*

<sup>29</sup>*Kamioka Observatory, Institute for Cosmic Ray Research, University of Tokyo, Kamioka, Gifu 506-1205, Japan*

<sup>30</sup>*Research Center for Cosmic Neutrinos, Institute for Cosmic Ray Research, University of Tokyo, Kashiwa, Chiba 277-8582, Japan*

<sup>31</sup>*TRIUMF, Vancouver, British Columbia V6T 2A3, Canada*

<sup>32</sup>*Instituto de Física Corpuscular, E-46071 Valencia, Spain*

<sup>33</sup>*Department of Physics, University of Washington, Seattle, Washington 98195-1560, USA*

<sup>34</sup>*Institute of Experimental Physics, Warsaw University, 00-681 Warsaw, Poland*

(Dated: October 26, 2018)

The atmospheric neutrino background for proton decay via  $p \rightarrow e^+\pi^0$  in ring imaging water Cherenkov detectors is studied with an artificial accelerator neutrino beam for the first time. In total,  $3.14 \times 10^5$  neutrino events corresponding to about 10 megaton-years of atmospheric neutrino interactions were collected by a 1,000 ton water Cherenkov detector (KT). The KT charged-current single  $\pi^0$  production data are well reproduced by simulation programs of neutrino and secondary hadronic interactions used in the Super-Kamiokande (SK) proton decay search. The obtained  $p \rightarrow e^+\pi^0$  background rate by the KT data for SK from the atmospheric neutrinos whose energies are below 3 GeV is  $1.63^{+0.42}_{-0.33}$  (stat.)  $^{+0.45}_{-0.51}$  (syst.) (megaton-year) $^{-1}$ . This result is also relevant to possible future, megaton-scale water Cherenkov detectors.

PACS numbers: 14.60.Pq, 13.15.+g, 25.30.Pt, 95.55.Vj

## I. INTRODUCTION

Discovery of nucleon decay would constitute direct evidence for grand unification of three fundamental forces [1, 2, 3] and point the way to a new theory beyond the standard model of elementary particle physics. Among many possible decay modes of nucleons, the decay mode  $p \rightarrow e^+\pi^0$  is dominant in a variety of such Grand Unified Theories (GUTs) [4, 5, 6].

The world's largest (22.5 kiloton fiducial volume) water Cherenkov detector experiment, Super-Kamiokande (SK) [7], has set a stringent partial lifetime limit of  $\tau/B_{p \rightarrow e^+\pi^0} > 5.4 \times 10^{33}$  years (90 % C.L.) for proton decays into  $e^+$  and  $\pi^0$  [8, 9, 10] based on the observation of no candidates in an integrated exposure of about 0.1 megaton-year (Mtyr). A  $p \rightarrow e^+\pi^0$  signal would be clearly identified in SK as showering Cherenkov rings corresponding to the positron and two gammas from  $\pi^0$  decay, with low net momentum and total invariant mass close to the proton mass. The estimated detection efficiency for the signal is 40 %, with a background rate of about 0.3 events in the integrated exposure predicted by the Monte Carlo simulation program (MC).

Characteristics of the background events from atmospheric neutrinos to SK's  $p \rightarrow e^+\pi^0$  search have been studied using MC [11]. Charged-current (CC) interactions of atmospheric  $\nu_e$  with only an electron and single  $\pi^0$  visible in the final state are the dominant source of the background. Neutral-current (NC) interactions with only two  $\pi^0$ 's visible in the final state are the remaining dominant background. Parent neutrino energies between 1 and 3 GeV dominate for both CC and NC background events. In this study, SK reports that about 24 % of the background events come from neutrinos above 3 GeV. The neutrino and final-state nuclear interactions are considered to be the dominant uncertainties for the background rate estimation. However, the background rate has been estimated only with MC without any quantitative systematic error estimation.

Some GUT models predict nucleon lifetimes just above the current limits, motivating proposals for future, megaton-scale SK-type water Cherenkov detector experiments [11, 12, 13, 14, 15, 16, 17]. Since SK and these more massive experiments would observe a non-negligible number of background events in the future, it is essential to check the predicted background rates experimentally.

In this study, neutrino and secondary hadronic interaction MCs used to estimate the background rate in SK proton decay searches are checked using muon neutrino beam data col-

lected with a 1,000 ton water Cherenkov detector (KT) in the K2K long-baseline neutrino oscillation experiment. The background rate for the  $p \rightarrow e^+\pi^0$  mode in SK and future megaton-scale water Cherenkov detectors is determined using the KT data.

While the KT measures muon neutrino reactions rather than electron neutrino reactions, the dynamics of pion production and re-scattering processes in the oxygen nucleus are identical between the two neutrino flavors. Therefore, rare CC  $\nu_e$  interaction topologies which may mimic proton decay can be checked using the KT  $\nu_\mu$  events with a muon and single  $\pi^0$  visible in the final state. The rate of the atmospheric CC  $\nu_e$  background can be determined using KT CC single  $\pi^0$  events with corrections for differences in neutrino flux and detection efficiency and the assumption that cross sections and final state kinematics for  $\nu_e$  and  $\nu_\mu$  are identical. In addition, the rate of the NC background can be determined with two  $\pi^0$ 's visible in the final state at the KT.

The number of  $\nu_\mu$  interactions in the KT is two orders of magnitude larger than previous data sets used for similar background studies using other types of detectors [18, 19, 20, 21]. The K2K beam is well matched to the atmospheric neutrino spectrum and samples the energies around a few GeV where most backgrounds arise. This is the first result of a proton decay background study using accelerator neutrino beam data collected with a water Cherenkov detector.

The outline of this paper is as follows: Section II reviews the K2K neutrino beam and the KT detector. Section III-A describes the data sample in the KT and validates the neutrino interaction models. Section III-B calculates the  $p \rightarrow e^+\pi^0$  background rate for proton decay detectors. Finally, Section IV concludes and summarizes these results.

## II. EXPERIMENTAL SETUP

### A. K2K neutrino beam

The wide-band neutrino beam used in the K2K long-baseline neutrino oscillation experiment [22] was primarily muon flavored (about 97.3, 1.3, and 1.5 % for  $\nu_\mu$ ,  $\nu_e$ , and  $\bar{\nu}_\mu$ , respectively) with a mean energy of 1.3 GeV. Protons accelerated by the KEK proton synchrotron to a kinetic energy of 12 GeV were extracted in a single turn to the neutrino beam line. The duration of an extraction, or “spill”, was 1.1  $\mu$ sec. The beam was transported to an aluminum target which was in the first of a pair of horn magnets. The horn system focused

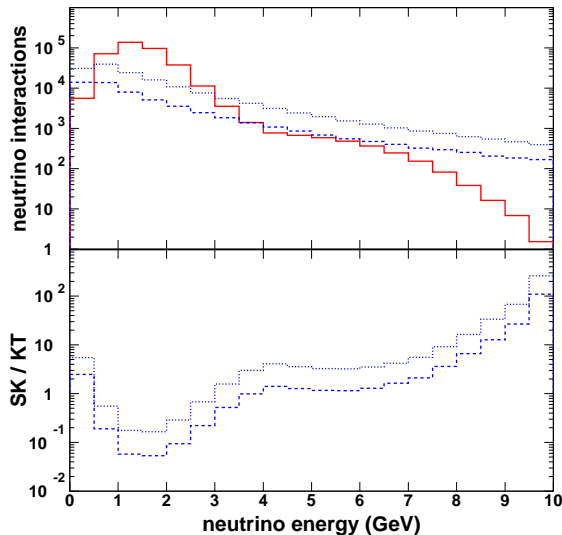


FIG. 1: The top figure compares the number of total  $\nu_\mu$  interactions in the KT 50 ton fiducial volume for  $7.4 \times 10^{19}$  protons on target (red solid) and the number of total neutrino interactions from atmospheric neutrinos in SK [24, 25] for 1 Mtyr exposure (blue dashed for  $\nu_e + \bar{\nu}_e$  and blue dotted for  $\nu_{all} + \bar{\nu}_{all}$ , where *all* stands for all the neutrino flavors). Disappearance of atmospheric  $\nu_\mu$ 's CC interactions due to neutrino oscillation is taken into account. The NEUT simulation program [26] is used for calculation of total neutrino interaction for each neutrino flavor. The bottom figure shows the ratio of neutrino energy spectra for the atmospheric neutrino interactions in SK and the K2K beam  $\nu_\mu$  interactions in KT. The meanings of the dashed and dotted lines are the same as above.

positive pions produced in proton-aluminum interactions into a 200 meter long decay volume. A beam dump was located at the end of the decay volume to absorb all surviving particles other than neutrinos. The neutrino beam's profile was measured using the distribution of neutrino interaction vertices in a muon range detector [23], one component of the K2K near neutrino detector system. The energy and angular distributions of muons from CC neutrino interactions were also continuously monitored.

Figure 1 compares total neutrino interaction (flux  $\times$  total cross section  $\times$  target volume  $\times$  time) spectra based on MC simulations for atmospheric neutrinos in SK [24, 25] with total  $\nu_\mu$  interaction spectra for the K2K beam in the KT detector, located 300 m downstream of the proton target. These total neutrino interaction spectra will be used for the background rate calculation shown in Sec. III-B-1. The neutrino spectrum measured by the KT covers the same energy range as the portion of the atmospheric neutrino spectrum which dominates the production of proton decay background events. Thus, analysis of the KT data allows a controlled study of the neutrino interaction channels and the nuclear re-scattering processes that determine the atmospheric neutrino backgrounds to nucleon decay in water Cherenkov detectors. In terms of the raw number of neutrino interactions between 1 and 3 GeV,

the KT  $\nu_\mu$  data correspond to about 10 Mtyr exposure to the atmospheric  $\nu_e$  flux at SK. A more complete relationship between the exposures will be derived in Sec. III-B-2.

## B. The 1000 ton water Cherenkov detector

The 1,000 ton ring imaging water Cherenkov detector (KT) was located in the K2K near detector hall. The KT was designed as a smaller replica of SK, using the same neutrino target material and instrumentation. The inner volume of KT was a cylinder 8.6 m in diameter and 8.6 m in height. This volume was viewed by 680 inward-facing 50 cm photomultiplier tubes (PMTs). The PMTs and their arrangement were identical to those of SK, covering 40 % of the detector's inner surface with active photo-cathode. The software-defined fiducial volume for this analysis, based on the reconstructed vertex for each neutrino interaction, is 50 tons in a 4 m by 4 m cylinder at the center of the tank, oriented along the beam axis. This fiducial volume is twice the standard fiducial volume (25 tons) used in other KT analyses [22, 27] in order to increase the statistics of the data set. Event selection within the fiducial volume results in a pure neutrino sample, with negligible contamination from cosmic rays and beam-induced muons entering the KT.

The KT data acquisition system was also similar to that of SK. The charge and timing information for each PMT hit above a threshold of approximately 1/4 photo-electron was digitized by custom electronics modules developed for SK [28]. The KT detector was triggered if there were more than 40 hit PMTs in a 200 ns timing window during the spill gate. The trigger threshold was roughly equivalent to the signal of a 6 MeV electron. The analog sum of all 680 PMTs' signals (PMTSUM) was also recorded during every spill by a 500 MHz FADC, to identify multiple neutrino interactions in a single spill. The number of interactions in a spill was determined by counting peaks in PMTSUM above a threshold equivalent to a 100 MeV electron. Only events with a single neutrino interaction in the spill, as determined by the PMTSUM peak search, are used in this study.

The KT and SK share a common library of event reconstruction algorithms [29] and detector simulation programs based on GEANT3 [30]. Similar detector calibration procedures are used in the KT [22] and SK, and similar detector performances are observed.

### 1. Event reconstruction performance

The KT event reconstruction performance parameters which are most relevant to this study are presented in this subsection. These reconstructions are used to select events and results of these performance studies are used to estimate systematic errors in this study.

A relativistic charged particle emits Cherenkov light in a cone with opening angle  $\cos^{-1}(1/n\beta) \sim 41^\circ$ , where  $n \sim 1.34$  is the refractive index for water, aligned with the particle's direction, and imaged as a ring by the detector's PMT

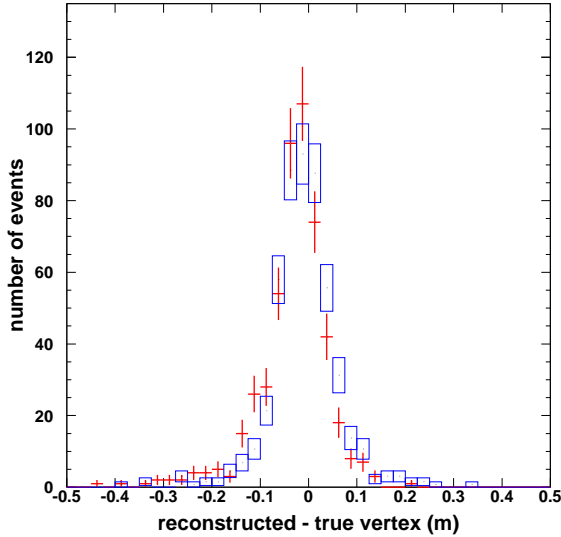


FIG. 2: Reconstructed - true vertex position of “cosmic ray pipe” muons entering at the center of KT. Red crosses (blue boxes) show the data (MC).

grid. Electrons and gammas generate electromagnetic showers (electrons also suffer multiple scatterings), which produce diffused ring patterns, while muons and charged pions create sharper ring images, with well-defined edges.

The interaction vertex for each event is reconstructed using PMT timing information. After fixing the vertex, the number of Cherenkov rings and their directions are determined by a maximum-likelihood procedure. The particle identification (PID) algorithm uses the charge pattern to classify each ring as a showering, electron-like particle ( $e^\pm$ ,  $\gamma$ ) or a non-showering, muon-like particle ( $\mu^\pm$ ,  $\pi^\pm$ ). For events with a single ring, charge information is used to refine the reconstructed vertex based on the PID result. Finally, the particle momentum of each ring is determined using charge information, based on the PID classification of the ring.

Vertex reconstruction in the KT was checked *in situ* with a special device called a “cosmic ray pipe”, which is a 25 cm diameter PVC pipe with scintillation counters at both ends. It was inserted from the top of the tank through a calibration access port near the center of the detector’s top wall. A coincidence between the two scintillation counters tagged a cosmic ray muon entering the detector at the lower end of the pipe. Such a muon has a known direction along the pipe and will begin radiating Cherenkov light when it leaves the pipe at a known location inside the detector. The “cosmic ray pipe” muon data were taken at five vertical positions: 0,  $\pm 1$ , and  $\pm 2$  m from the center of the fiducial volume. Figure 2 shows a typical reconstructed vertex distribution of “cosmic ray pipe” muons. The vertex resolution along the vertical direction was 10 cm or better, and the central values of the distributions for data and MC agree within 4 cm for all test points. The events in Fig. 2 have had a vertex refinement based on charge and PID information applied to them. The vertex resolution for

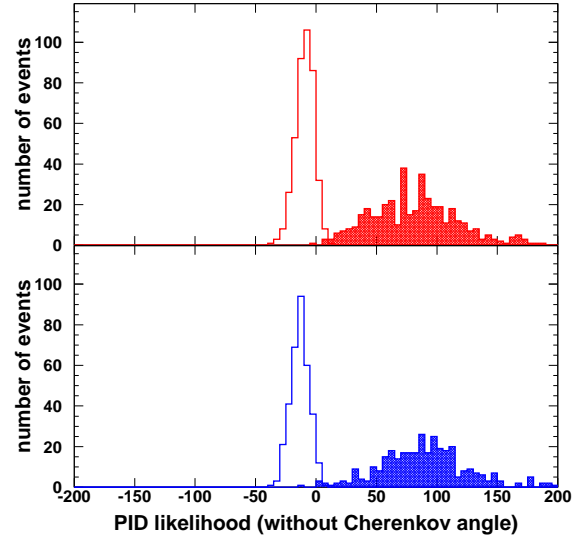


FIG. 3: PID likelihood for cosmic ray muons (shaded histogram) and the decay electrons (open histogram). The red (blue) histogram (top (bottom) figure) shows data (MC). Positive (negative) likelihood corresponds to muon (electron)-like.

multi-ring decays without this refinement, such as simulated  $p \rightarrow \mu^+ \pi^0$  signal events, is 28 cm.

The PID performance is checked with cosmic ray muons and their associated decay electrons. As shown in Fig. 3, the PID likelihood distributions are clearly separated between the two types of rings, although note that the momenta of particles from the proton decay is typically higher than that of Michel electrons. Mis-ID probabilities for 500 MeV/c muons and electrons were estimated with Monte Carlo to be 0.5 % and 0.8 %, respectively.

Figure 4 shows momentum loss, as estimated by reconstructed momentum divided by measured range, for stopping cosmic ray muons. The stopping point of a muon is determined by the reconstructed vertex of its decay electron. Both vertical stopping muons which enter from the top of the tank toward the bottom direction and horizontal stopping muons entering from one side of the barrel toward the other are shown in Fig. 4. The largest difference (3 %) between data and MC comes from the horizontal muons, and is used in the estimate of the absolute energy scale uncertainty. The difference (1.7 %) between vertical and horizontal muons is used to estimate the detector asymmetry of the energy scale. The directional dependence of reconstructed momentum of Michel electrons is also checked and found to be uniform within the statistical error (2.4 %) of the sample. Figure 5 shows the reconstructed invariant mass of NC single- $\pi^0$  events induced by the neutrino beam [27]. The events must be fully-contained (deposit all of their Cherenkov light inside the inner detector) and have two electron-like rings. The  $\pi^0$  mass peak is clearly observed, but shifted slightly higher than the nominal value of 135 MeV/c<sup>2</sup>. This shift is the result of energy deposit from de-excitation  $\gamma$ ’s from oxygen nuclei in neutrino interac-

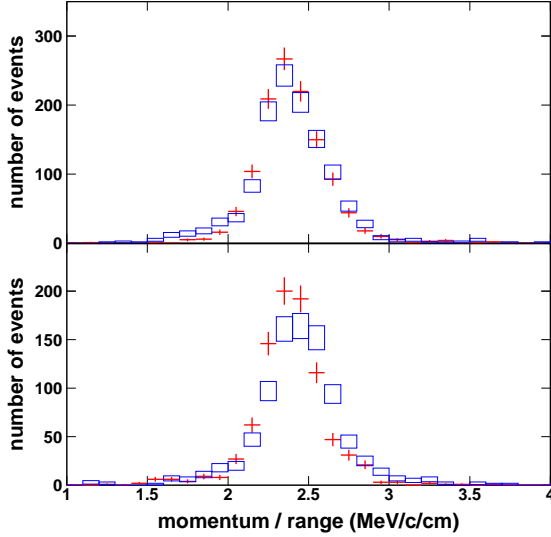


FIG. 4: Reconstructed momentum divided by range for vertical (top figure) and horizontal (bottom) cosmic ray muons. Red crosses (blue boxes) show the data (MC).

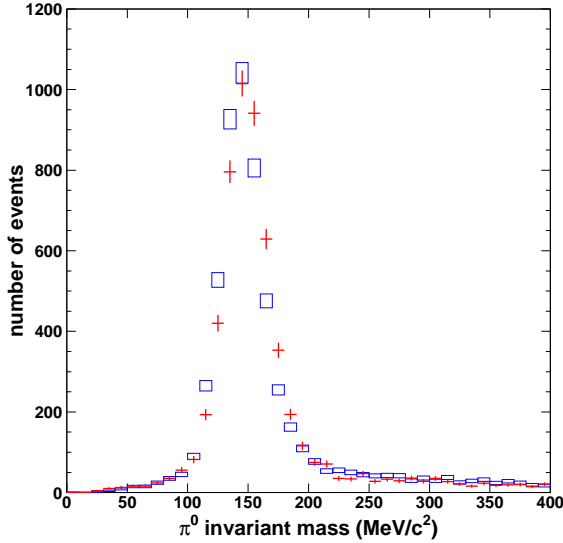


FIG. 5: Reconstructed mass of  $\pi^0$  candidates produced by NC interactions in the K2K beam. Red crosses (blue boxes) show the data (MC).

tions as well as a bias in the  $\gamma\gamma$  opening angle due to known vertex reconstruction bias. Each effect is several MeV and is included in MC. The remaining difference between data and MC is 4 % by comparing the  $\pi^0$  mass peaks, and is also used to estimate the absolute energy scale uncertainty. Taking these measurements together, the absolute energy scale uncertainty is determined to be  $^{+3}_{-4}$  % from the horizontal stopping cosmic ray muon and  $\pi^0$  samples, and the detector asymmetry of the

energy scale is 1.7 %. The absolute energy scale was stable within 1 % over the period when data for the present study were collected.

### III. DATA ANALYSIS

All available good quality KT data from the 2000–2004 K2K running periods were used in this analysis. In this period,  $3.14 \times 10^5$  total neutrino events ( $2.75 \times 10^5$  events with a single neutrino interaction in a spill) in the 50 ton fiducial volume, corresponding to  $7.4 \times 10^{19}$  protons on target (pot), were collected.

#### A. Validation of neutrino interaction simulations

Several packages to simulate neutrino interactions have been developed [31]. Both the NEUT [26] and NUANCE [32] simulation programs have been used in SK to estimate the background rates for nucleon decay searches. These programs have already been used for various physics analyses and confirmed to reproduce data well [22, 25, 27]. In this analysis, the neutrino-induced  $\mu^+\pi^0$  sample is used to do a careful comparison of the rates and distributions relevant to the  $p \rightarrow e^+\pi^0$  search.

##### 1. Data and MC event selection criteria

CC  $\nu_\mu$  interactions producing only a muon and single  $\pi^0$  visible in the final state (“ $\mu\pi^0$ ” events) can, except for the choice of lepton PID, be selected in the KT with nearly the same cuts used for the SK  $p \rightarrow e^+\pi^0$  search:

##### (A) Fully-contained (FC):

The FC criterion in the KT detector requires that no PMT signal greater than 200 photo-electrons is recorded, since charged particles leaving the detector produce a large signal in the PMT around their exit point.

##### (B) Two or three identified rings:

At the neutrino energies relevant to this study, recoiling protons are usually invisible because they are below Cherenkov threshold. Events with both two and three rings are accepted because, in some cases, one of the two gammas from the  $\pi^0$  decay is missed during reconstruction. This can happen when the decay is very asymmetric in energy, or the rings are too close to resolve.

##### (C) PID:

One identified ring must be muon-like and the other one or two rings must be electron-like.

##### (D) $\pi^0$ mass:

For three-ring events, the reconstructed invariant mass of the two electron-like rings must be between 85 and 215  $\text{MeV}/c^2$ .

The SK  $p \rightarrow e^+\pi^0$  selection criteria are identical, except that the outer detector information is used to select the FC events, all rings must be electron-like, and events with one or more identified muon decays are rejected.

Finally, the proton decay signal box defines a “ $p \rightarrow \mu\pi^0$ ” sub-sample of “ $\mu\pi^0$ ” events consistent with the proton mass (about 1 GeV/c<sup>2</sup>) and Fermi motion in oxygen. The oxygen nucleus is modeled with as a relativistic Fermi gas with the Fermi surface momentum set to about 220 MeV/c. The selection criteria used are:

(E) *Proton decay kinematics:*

Total momentum  $P_{tot}$  must be less than 250 MeV/c and total invariant mass  $M_{tot}$  must be between 800 and 1050 MeV/c<sup>2</sup>, where:

- $P_{tot} \equiv |\sum_i \vec{p}_i|$ ,
- $M_{tot} \equiv \sqrt{E_{tot}^2 - P_{tot}^2}$ ,
- $E_{tot} \equiv \sum_i \sqrt{|\vec{p}_i|^2 + m_i^2}$ ,
- $\vec{p}_i$  is the reconstructed momentum vector of the  $i$ -th ring, and
- $m_i$  is the mass of the particle corresponding to the  $i$ -th ring inferred from PID (either gamma or muon).

Figure 6 shows the event display of “ $p \rightarrow \mu\pi^0$ ” sample in the KT real data falling within the proton decay signal box. Three Cherenkov rings are clearly visible and well reconstructed.

## 2. MC data samples

MC  $\nu_\mu$  data samples corresponding to  $1.1 \times 10^{20}$  pot and  $5.4 \times 10^{19}$  pot were generated by NEUT and NUANCE, respectively, and fully reconstructed after full simulation of detector response using GEANT. These MC samples are used to generally study the “ $\mu\pi^0$ ” events. To extensively investigate events in the proton decay signal box, additional  $\nu_\mu$  interactions were generated with NEUT for 1.4, 5.0, 32.4, 54.0, and  $35.9 \times 10^{21}$  pot in neutrino energy bins 0–2.5, 2.5–3, 3–4, 4–5, and 5–6 GeV, respectively. This additional sample was preselected before reconstruction, using loose cuts on the total charge and charge anisotropy from the generated vertex. The breakdown of events surviving the selection criteria into different reaction channels for the NEUT sample is summarized in Tbl. I. Resonant CC single pion production dominates both the “ $\mu\pi^0$ ” and “ $p \rightarrow \mu\pi^0$ ” samples. The quasi-elastic contribution arises through production of  $\pi^0$  by recoil nucleon interactions with H<sub>2</sub>O (also simulated by the GEANT and CALOR [33] packages). Identification of charged pions as muons by the PID is the dominant source of the NC fraction.

Figure 7 shows that the rates of events surviving after each selection (A–E) for data and both MC samples agree well. The simulated data are normalized by the number of total neutrino interactions in the 25 ton fiducial volume [22] in this plot.

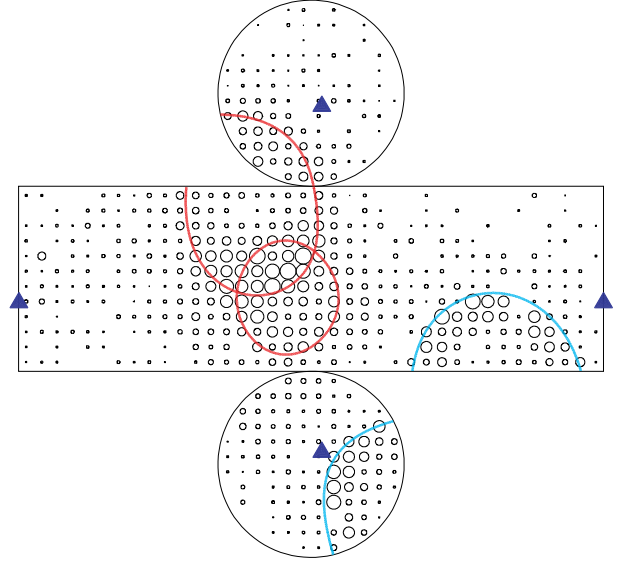


FIG. 6: Event display of “ $p \rightarrow \mu\pi^0$ ” sample in the KT real data satisfying selection criteria (A)–(E). Each hit PMT is represented by a small circle whose area is proportional to the PMT’s measured charge. The small blue triangles show the projection of the reconstructed vertex onto the walls. Cyan (red) thick circles show reconstructed rings identified by the PID as muon (electron)-like (Two overlapped thick circles are identified as electron-like rings). The reconstructed  $M_{\pi^0}$ ,  $M_{tot}$ , and  $P_{tot}$  for this event are 164 MeV/c<sup>2</sup>, 851 MeV/c<sup>2</sup>, and 226 MeV/c, respectively.

Event category	(A)-(D) (%)	(A)-(E) (%)
	“ $\mu\pi^0$ ” sample	“ $p \rightarrow \mu\pi^0$ ” sample
CC quasi elastic	12.2±0.2 (4.3±0.2)	18.6±1.9
CC single pion from resonance	50.2±0.3 (48.7±0.6)	60.4±2.4
CC multi pions	22.2±0.3 (29.9±0.5)	16.1±1.8
CC deep inelastic scattering	0.6±0.1 (0.5±0.1)	1.0±0.5
NC	14.8±0.2 (16.5±0.4)	4.0±1.0

TABLE I: NEUT abundance of different reaction channels [26] after applying event selections (A)–(D) and (A)–(E). Note that hadron system invariant mass  $W$  is different for “multi pions” and “deep inelastic scattering” modes as  $1.3 \leq W \leq 2.0$  GeV and  $W \geq 2.0$  GeV, respectively. “NC” includes all the modes shown for “CC”. The errors shown are MC statistical. The number in parentheses for (A)–(D) shows the population for events with three identified rings only.

For the data, 24 events remain in the proton decay signal box for  $7.4 \times 10^{19}$  pot, while  $21.4 \pm 3.8$  (stat) and  $13.6 \pm 4.4$  (stat) are expected from NEUT and NUANCE, respectively, for the same number of total neutrino interactions in the 25 ton fiducial volume.

All simulated events in the proton decay signal box were inspected, and about 90 % show a correctly reconstructed, back-to-back muon and  $\pi^0$  from the CC neutrino interactions. The remaining 10 % mostly result from identification of a proton as a gamma, or a charged pion as a gamma or a muon. This remaining fraction is used to estimate the systematic error on



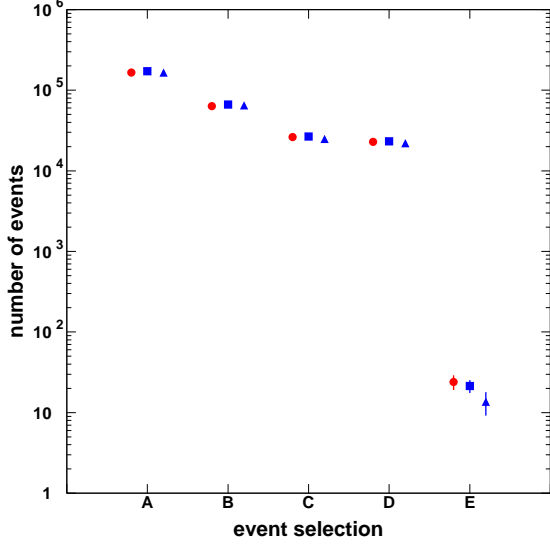


FIG. 7: Event rate after application of each selection criterion. The event selections (A)-(E) are explained in text. The event rates at D and E correspond to “ $\mu\pi^0$ ” and “ $p \rightarrow \mu\pi^0$ ” samples, respectively. The data, NEUT, and NUANCE are shown as red circles, blue squares, and blue triangles, respectively. The simulated data are normalized by the total number of neutrino interactions in the 25 ton fiducial volume.

the efficiency difference between SK and KT shown in Tbl. II.

In the MC, 98 % of “ $p \rightarrow \mu\pi^0$ ” events found in the signal box are from neutrinos interacting with nucleons in the oxygen nucleus. The remaining 2 % of events are from neutrinos interacting with free protons where a  $\pi^0$  is produced by hadronic interaction of the struck nucleon with  $H_2O$ .

### 3. Comparison of kinematics between data and MC

Since the background for proton decay searches depends not only on the neutrino interaction rate but also on the event topologies, it is important to verify that the simulations correctly reproduce the kinematics of each particle in the final state. Resonant single-pion production, which is the dominant source of the background, can be characterized by the momentum transfer  $Q^2$  and the invariant mass of the hadronic system  $W$ . Assuming a resonance-mediated three-body reaction ( $\nu_\mu n \rightarrow \mu^- A, A \rightarrow p\pi^0$ ) and neglecting the Fermi motion and binding energy of the target, the kinematic variables of interest can be reconstructed from the observable quantities:

$$W^2 = \frac{(E_\pi - p_\pi \cos \theta_\pi)(2m_n E_\mu - m_n^2 - m_\mu^2) + (2m_n E_\pi - 2E_\mu E_\pi + 2p_\mu p_\pi \cos \theta_{\mu\pi} + m_p^2 - m_\pi^2)(m_n - E_\mu + p_\mu \cos \theta_\mu)}{(m_n - E_\mu + p_\mu \cos \theta_\mu - E_\pi + p_\pi \cos \theta_\pi)},$$

and

$$Q^2 = 2E_\nu(E_\mu - p_\mu \cos \theta_\mu) - m_\mu^2,$$

in natural units where  $p$ ,  $\theta$ ,  $m$ , and  $E$  are a given particle’s reconstructed momentum, reconstructed angle from the beam direction, mass, and calculated energy, respectively, and  $\theta_{\mu\pi}$  as the angle between reconstructed muon and  $\pi^0$  directions. Also,

$$E_\nu = \frac{2m_n E_\mu + W^2 - m_n^2 - m_\mu^2}{2(m_n - E_\mu + p_\mu \cos \theta_\mu)}$$

is the inferred neutrino energy where “ $\pi$ ”, “ $n$ ”, “ $\mu$ ”, and “ $p$ ” in these formulas stand for  $\pi^0$ , neutron,  $\mu^-$ , and proton, respectively.

Figs. 8 and 9 show the reconstructed hadronic mass  $W$  and momentum transfer  $Q^2$  of three ring “ $\mu\pi^0$ ” events. Uncertainties in the KT event reconstruction are accounted for in the real data points as correlated systematic errors, so the error bars shown on each bin are not independent. Although there may be a slight excess at small  $Q^2$  in NUANCE, the agreement between data and both MC samples is good for both kinematic variables within the measurement errors.

The kinematic variables  $Q^2$  and  $W$  do not translate directly into the quantities  $M_{tot}$  vs.  $P_{tot}$  used as the final selection for proton decay candidates, so it is important to check the latter as well. Figure 10-12 show the distributions of  $P_{tot}$  vs.  $M_{tot}$  for all “ $\mu\pi^0$ ” events from data, NEUT, and NUANCE, respectively.

To simplify comparison between data and MC samples, one dimensional projections of  $M_{tot}$  for  $P_{tot} \leq 250$  MeV/ $c$  and  $P_{tot}$  for  $800 \leq M_{tot} \leq 1050$  MeV/ $c^2$  are shown in Fig. 13 and Fig. 14, respectively. Note that omitted statistical errors on the MC samples are almost the same as those on data. Also, a metric quantifying an event’s distance from the center of the signal box is introduced:  $L \equiv \sqrt{X^2 + Y^2}$ , where

$$\begin{aligned} X &\equiv M_{tot}c^2 - 938 \text{ MeV} \\ Y &\equiv \begin{cases} P_{tot}c - 200 \text{ MeV} & (P_{tot} > 200 \text{ MeV}/c) \\ 0 & (P_{tot} \leq 200 \text{ MeV}/c) \end{cases} \end{aligned}$$

The  $L$  distributions for data and MC samples are plotted in Fig. 15. The data and both simulations agree well, within measurement errors, for all values of  $M_{tot}$  (Fig. 13),  $P_{tot}$  (Fig. 14), and  $L$  (Fig. 15), including the tails of distributions where the proton decay signal box is located.

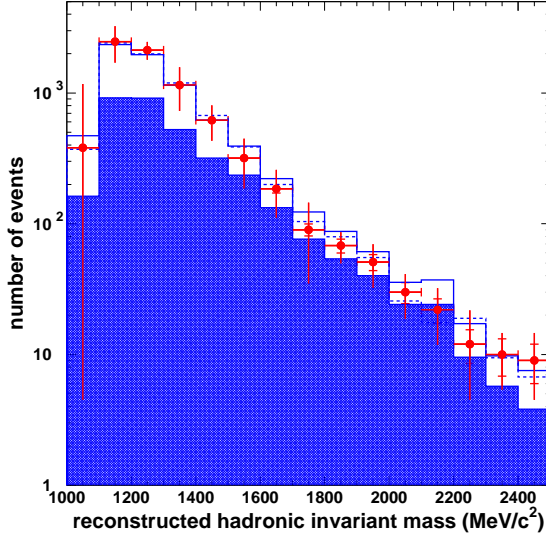


FIG. 8: Reconstructed hadronic invariant mass  $W$  for three ring “ $\mu\pi^0$ ” events, assuming CC single  $\pi^0$  production via resonance. Red crosses show the data with statistical and total measurement errors. The relatively large systematic errors in this plot are correlated between bins, and arise from the absolute energy scale uncertainty. The NEUT (NUANCE) prediction is shown by the solid (dashed) blue histogram. The hatched histogram shows the distribution of NEUT events that originate from resonant CC single pion production. Both MC samples are normalized to the data by number of entries.

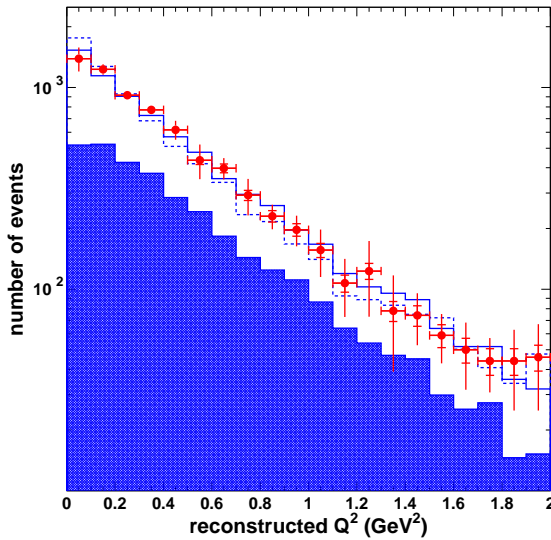


FIG. 9: Reconstructed momentum transfer  $Q^2$  for three ring “ $\mu\pi^0$ ” events, assuming CC single  $\pi^0$  production via resonance. Red crosses show the data with statistical and total measurement errors. The NEUT (NUANCE) prediction is shown by the solid (dashed) blue histogram. The hatched histogram shows the distribution of NEUT events that originate from resonant CC single pion production. Both MC samples are normalized to the data by number of entries.

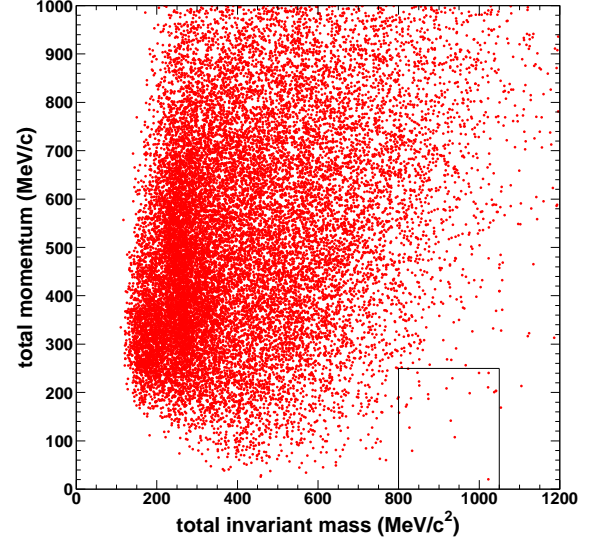


FIG. 10: Total momentum  $P_{tot}$  vs. total invariant mass  $M_{tot}$  for “ $\mu\pi^0$ ” events from the KT data ( $7.4 \times 10^{19}$  pot), with the proton decay signal box superimposed.

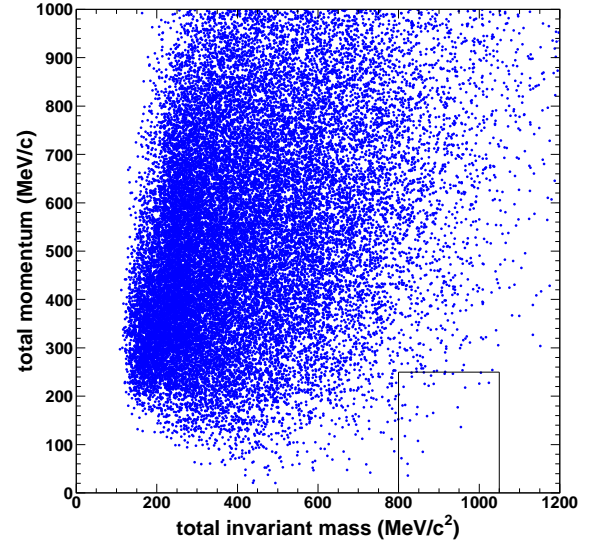


FIG. 11: Total momentum  $P_{tot}$  vs. total invariant mass  $M_{tot}$  for “ $\mu\pi^0$ ” events from NEUT ( $1.1 \times 10^{20}$  pot), with the proton decay signal box superimposed.

In summary, these comparisons show good agreement between data and MC samples; hence, the modeling of neutrino and final-state nuclear interactions relevant to  $p \rightarrow e^+\pi^0$  backgrounds appears to be well supported by the KT data.



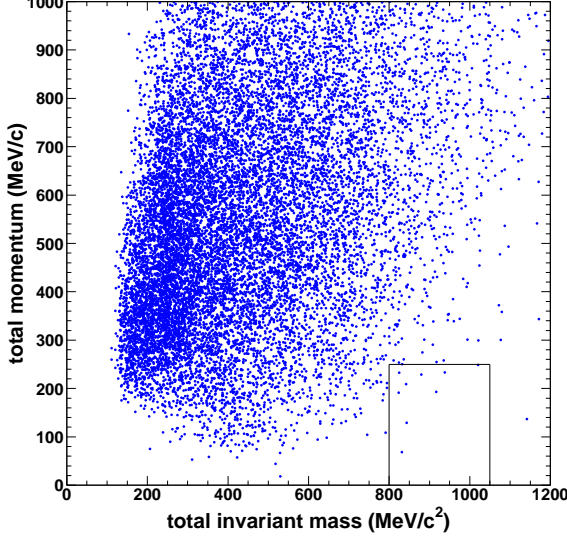


FIG. 12: Total momentum  $P_{tot}$  vs. total invariant mass  $M_{tot}$  for “ $\mu\pi^0$ ” events from NUANCE ( $5.4 \times 10^{19}$  pot), with the proton decay signal box superimposed.

## B. Determination of the background rate to the $p \rightarrow e^+\pi^0$ search

### 1. General method

Predicting the background rate for the  $p \rightarrow e^+\pi^0$  search requires extrapolation from the KT  $\nu_\mu$  beam data to all flavors of the atmospheric neutrino flux, and re-weighting the K2K neutrino spectrum to match the atmospheric neutrino flux and spectrum. The CC background event rate from  $\nu_e$  is obtained using lepton universality, the assumption that the cross sections and final state kinematics for  $\nu_e$  and  $\nu_\mu$  are nearly identical. The NC background rate is directly measured. The anti-neutrino background rate for all flavors is estimated by rescaling the  $\nu_\mu$  data to the predicted total event rates for each anti-neutrino. Anti-neutrino final-states tend to have smaller  $Q^2$  due to the different fraction of neutrino energy transferred to the hadronic system in inelastic reactions and therefore tend to have a larger momentum imbalance between the lepton and hadronic systems. Simulated data samples confirm that anti-neutrinos are less likely than neutrinos to fall within the signal box, so the rescaling procedure is conservative.

The expected event rate of the  $p \rightarrow e^+\pi^0$  background for general water Cherenkov detectors,  $N$ , can be expressed as:

$$N = n^{CC} \cdot R_\phi^{CC} \cdot R_\epsilon^{CC} + n^{NC} \cdot R_\phi^{NC} \cdot R_\epsilon^{NC}, \quad (1)$$

where the 1st (2nd) term corresponds to the background rate coming from the CC (NC) neutrino interactions,  $n$  is the observed events in the proton decay signal box at the KT, and  $R_\phi$  is a ratio of total neutrino interactions (flux  $\times$  total cross section  $\times$  target volume  $\times$  time) between the atmospheric neutrinos at the proton decay detectors and the K2K muon neutrinos.

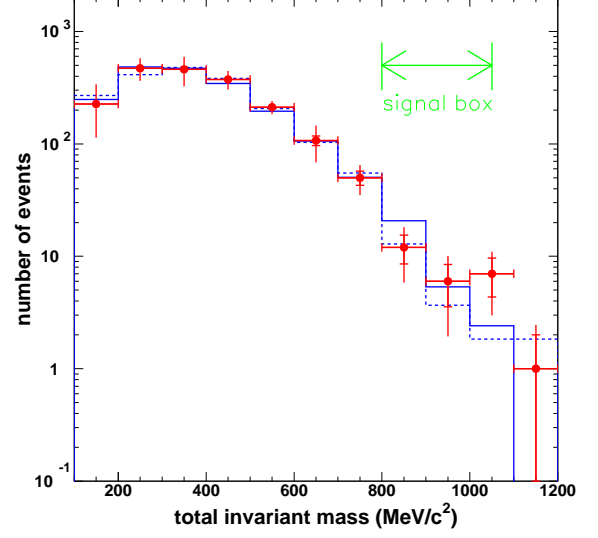


FIG. 13: Total invariant mass  $M_{tot}$  for “ $\mu\pi^0$ ” events with total momentum  $P_{tot} \leq 250$  MeV/c. Red crosses show the data with statistical and total measurement errors. The NEUT (NUANCE) predictions are shown by a solid (dashed) blue histogram. Both MC samples are normalized to the data by number of entries. The green arrow shows the range accepted by the proton decay signal box.

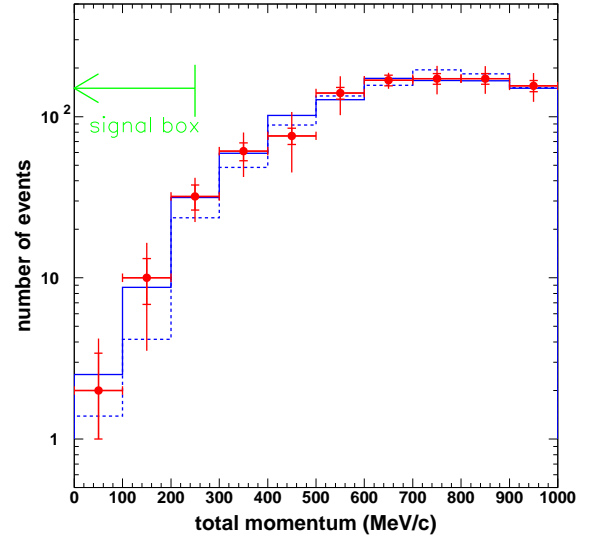


FIG. 14: Total momentum  $P_{tot}$  for “ $\mu\pi^0$ ” events with total invariant mass  $800 \leq M_{tot} \leq 1050$  MeV/c<sup>2</sup>. Red crosses show the data with statistical and total measurement errors. The NEUT (NUANCE) predictions are shown by a solid (dashed) blue histogram. Both MC samples are normalized to the data by number of entries. The green arrow shows the range accepted by the proton decay signal box.

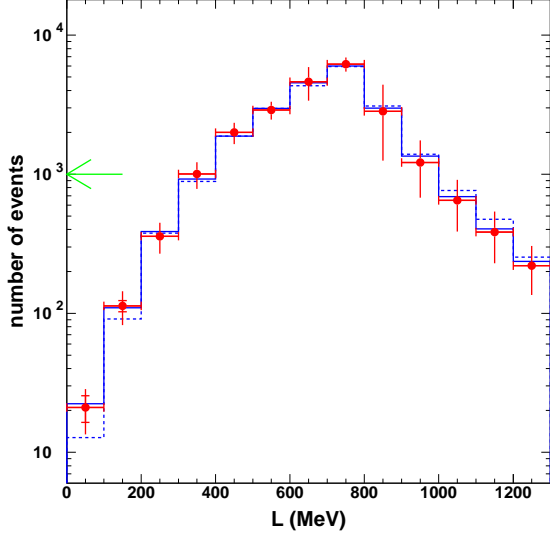


FIG. 15:  $L$  (as defined in the text) for “ $\mu\pi^0$ ” events. Red crosses show the data with statistical and total measurement errors. The NEUT (NUANCE) predictions are shown by a solid (dashed) blue histogram. Both MC samples are normalized to the data by number of entries. The green arrow indicates the range accepted by the proton decay signal box.

nos at the KT. In using Eqn. 1,  $\nu_e + \bar{\nu}_e$  and  $\nu_{all} + \bar{\nu}_{all}$  (where *all* stands for all the neutrino flavors) are used for the atmospheric neutrino flux for the CC and NC background measurements, respectively.  $R_\phi$  is essentially an energy-dependent flux correction factor, multiplied by an overall scale factor based on the respective target masses and exposure. Finally,  $R_\epsilon$  is the ratio of detection probabilities for the background events at the proton decay detectors and the KT. Any difference in detection efficiency between the “ $p \rightarrow e\pi^0$ ” sample in the proton decay detectors and the “ $p \rightarrow \mu\pi^0$ ” sample in the KT is reflected in  $R_\epsilon^{CC}$ .

Since the numbers of “ $p \rightarrow \mu\pi^0$ ” events from NEUT and NUANCE at KT are statistically consistent with each other, one (NEUT) of the models is chosen for the background rate determination in this study.

As shown in Sec. III-A-2, the remaining number of “ $\mu\pi^0$ ” events in the proton decay signal box,  $n^{CC}$ , is 24 for  $7.4 \times 10^{19}$  pot.

The number of NC background events, the NC interactions with only two  $\pi^0$ s visible in the final state, is measured with the KT by applying the same event selection criteria used in the SK  $p \rightarrow e^+\pi^0$  search. The events must be fully-contained, and have two or three rings, all of which must be electron-like. For three-ring events, there must be a reconstructed  $\pi^0$  mass between 85 and 215 MeV/ $c^2$ . The total mass of the event must satisfy the conditions  $800 \leq M_{tot} \leq 1050$  MeV/ $c^2$ , and the  $P_{tot} \leq 250$  MeV/ $c$ .

In the SK data analysis, a decay-electron cut is also applied to the data and MC samples. The reconstruction software used at the KT during K2K running did not implement a decay-

electron cut. However, it was found that the NC background rate was so small after the previous cuts that there were no data candidates left to check for muon-decays. For the KT MC “ $p \rightarrow e\pi^0$ ” sample, a cut was applied using the MC truth information assuming the same decay-electron finding efficiency as SK. With the exceptions of the decay-electron cut and method for FC event selection, which in SK employs the outer detector, the selection criteria applied for these two detectors are identical.

No candidates of the “ $p \rightarrow e\pi^0$ ” events are found in the KT data ( $n^{NC} = 0$  for  $7.4 \times 10^{19}$  pot), while the expected number of NC events is  $0.30 \pm 0.13$  (stat.) for the same number of total neutrino interactions in the 25 ton fiducial volume. All the MC “ $p \rightarrow e\pi^0$ ” events from the NC interactions are found to have only two  $\pi^0$ s visible in the final state. These events were NC single pion resonance events with an extra pion produced by hadronic interactions in the water.

## 2. Application to Super-Kamiokande-I

In order to calculate the background to the proton decay search at the SK-I experiment [9, 10] the interaction rates are first re-weighted to the atmospheric flux in SK [24, 25] and the SK fiducial volume of 22.5 kiloton and used to calculate:

$$R_\phi^{CC(NC)} = \frac{\sum_i^{energy \text{ bins}} m_i^{CC(NC)} \cdot r_{\phi i}^{CC(NC)}}{\sum_j^{energy \text{ bins}} m_j^{CC(NC)}}, \quad (2)$$

where  $m^{CC(NC)}$  is the expected number of “ $p \rightarrow \mu(e)\pi^0$ ” events from CC(NC) interactions in the KT for  $7.4 \times 10^{19}$  pot and  $r_\phi^{CC(NC)}$  is the expected ratio of  $\nu_e + \bar{\nu}_e$  ( $\nu_{all} + \bar{\nu}_{all}$ ) interactions in SK for 1 Mtyr to the  $\nu_\mu$  interactions in the KT.  $r_\phi^{CC(NC)}$  and  $m^{CC(NC)}$  are shown in Fig. 1 (bottom) and Fig. 16, respectively.

The background rate is estimated only for  $E_\nu < 3$  GeV in this study since the expected number of “ $p \rightarrow \mu(e)\pi^0$ ” events in the KT is small ( $< 10^{-1}$ ) above 3 GeV as shown in Fig. 16. The obtained results for  $E_\nu < 3$  GeV are  $R_\phi^{CC} = (15.9 \text{ Mtyr})^{-1}$  and  $R_\phi^{NC} = (4.5 \text{ Mtyr})^{-1}$ . For example,  $R_\phi^{CC} = (15.9 \text{ Mtyr})^{-1}$  means that KT  $\nu_\mu$  data corresponds to 15.9 Mtyr exposure of the atmospheric neutrino data of the CC background events at SK. The difference between  $R_\phi^{CC}$  and  $R_\phi^{NC}$  mostly comes from the difference between  $r_\phi^{CC}$  and  $r_\phi^{NC}$ . The fraction of background events above 3 GeV in a search for  $p \rightarrow e^+\pi^0$  at SK is reported to be about 24 % using MC [11].

The efficiency ratio for the background events,  $R_\epsilon^{CC(NC)}$ , can be estimated by using proton decay signal MC (note that the majority of the background events really have visible Cherenkov rings and their kinematics are consistent with proton decay signals as shown in Sec. III-A-2):  $R_\epsilon^{CC(NC)} = \epsilon / \epsilon^{CC(NC)}$ , where  $\epsilon = 0.40$  is the efficiency for  $p \rightarrow e^+\pi^0$  MC events at SK and  $\epsilon^{CC(NC)} = 0.37(0.34)$  are the efficiencies for  $p \rightarrow \mu^+\pi^0$  and  $p \rightarrow e^+\pi^0$  MC events in the KT. The largest source of inefficiency for both detectors is due to final-state

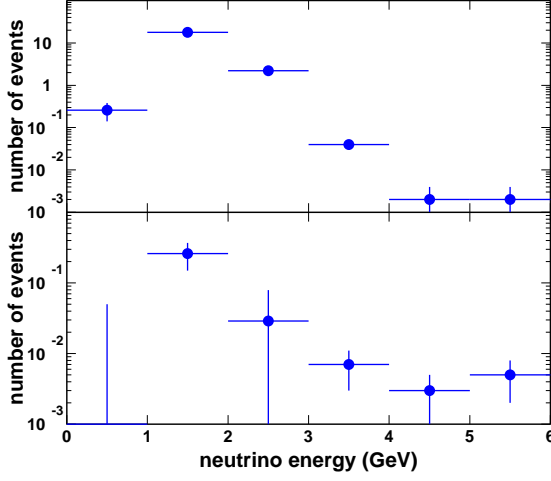


FIG. 16: Predicted number of CC ( $m^{CC}(i)$  shown in top) and NC ( $m^{NC}(i)$  shown in bottom) “ $p \rightarrow \mu(e)\pi^0$ ” events from NEUT in the KT for  $7.4 \times 10^{19}$  pot, in bins of true parent neutrino energy  $i$ . The errors shown are MC statistical.

pion interactions in the oxygen nucleus. The efficiencies for free protons are 0.80 and 0.77 for  $p \rightarrow e^+\pi^0$  MC events at SK and  $p \rightarrow \mu^+\pi^0$  MC events in the KT, respectively. The 15 % ( $=0.34/0.40$ ) difference between SK and KT efficiencies for  $p \rightarrow e^+\pi^0$  is mainly due to the different FC selection criterion.

Finally, using the numbers above the atmospheric neutrino background rate for the SK  $p \rightarrow e^+\pi^0$  search,  $N$ , is determined to be:

$$\begin{aligned} N \text{ (Mtyr}^{-1}\text{)} &= \{1.63 \pm 0.33(\text{stat.})^{+0.43}_{-0.51}(\text{syst.})\}(\text{CC}) \\ &\quad + \{0.00 + 0.26(\text{stat.}) + 0.13(\text{syst.})\}(\text{NC}) \\ &= 1.63^{+0.42}_{-0.33}(\text{stat.})^{+0.45}_{-0.51}(\text{syst.}). \end{aligned}$$

Table II summarizes the systematic errors on each parameter in Eqn. (1). Uncertainties from the performance of the KT reconstruction are reflected in the error on  $n^{CC}$ . The error is estimated by evaluating the effect of reconstruction uncertainties on the number of  $p \rightarrow \mu^+\pi^0$  MC events in the proton decay signal box. To account for the NC contamination in the “ $p \rightarrow \mu\pi^0$ ” CC events (Tbl. I), an asymmetric error of (+0/-4 %) is assigned to  $n^{CC}$ . It was not necessary to estimate the errors on  $n^{NC}$  as there was no observation of “ $p \rightarrow e\pi^0$ ” events in the KT. The expected event rate in this case is much smaller than that from the CC events, which dominates the background.

One (15 %) of the dominant errors on  $R_\phi^{CC}$  comes from uncertainty of total neutrino interactions with atmospheric neutrino flux at SK. The cross section systematic errors considered are 10 % on the axial vector masses for quasi-elastic and single-pion production, 10 % on the total cross sections for quasi-elastic and single-pion production, 5 % on the total

Error source	error on $n^{CC}$ (%)
KT vertex reconstruction	3
KT absolute energy scale	3
KT detector asymmetry of energy scale	3
KT FC event selection	1
KT ring counting	9
KT ring direction	3
KT PID	9
KT NC fraction in “ $p \rightarrow \mu\pi^0$ ” events	+0/-4
Sub total	+14/-15

Error source	error on $R_\phi^{CC(NC)}$ (%)
K2K flux shape	3(6)
K2K beam $\nu_e$ contamination	<1(5)
KT MC normalization	4(4)
KT MC statistics	5(47)
atmospheric $\nu$ flux [24, 25]	10(10)
total $\nu$ cross section ratio	15(15)
lepton universality	<1(0)
atmospheric anti- $\nu$ rate	+0/-16(6)
Sub total	+25/-29(54)

Error source	error on $R_\epsilon^{CC(NC)}$ (%)
Efficiency difference between SK and the KT	11(7)

TABLE II: Summary of systematic errors for measurement of the background rate to the  $p \rightarrow e^+\pi^0$  search.

cross section for deep-inelastic scattering, with and without correction of the nuclear structure functions for deep-inelastic scattering (Bodek & Yang correction [34]), and 20 % on the ratio of NC/CC cross sections. The other dominant error (+0/-16 %) on  $R_\phi^{CC}$  comes from differences in kinematics of the final-state particles between neutrinos and anti-neutrinos. The error on  $R_\phi^{CC}$  ( $R_\phi^{NC}$ ) is estimated by comparing the number of simulated CC single- $\pi^0$  (NC two- $\pi^0$ ) events near the signal box. The error on  $R_\phi^{CC}$  from the lepton universality assumption is estimated by comparing the number of CC single- $\pi^0$  events near the signal box using simulated  $\nu_\mu$  and  $\nu_e$  interactions and is found to be negligibly small. The largest error (47 %) on  $R_\phi^{CC}$  arises from the statistics of simulated “ $p \rightarrow e\pi^0$ ” events ( $m^{NC}$  in Eqn. (2)) in the KT. The KT MC data are normalized by the number of total neutrino interactions observed in the 25 ton fiducial volume. The estimate of the error on the fiducial volume is 4 % [22].

The systematic error on  $R_\epsilon^{CC(NC)}$  is estimated by taking into account the differences of PID performance between SK and the KT and the mis-identification probability of charged pions or protons as either muons or gammas in the KT MC sample.

### 3. Discussions

A total of 2.14 ( $=1.63/0.76$ , where 0.76 is fraction of the background events below 3 GeV at SK[11]) atmospheric neutrino background events are expected for 1 Mtyr for SK-type water Cherenkov detectors. If the proton lifetime  $\tau/B_{p \rightarrow e^+\pi^0}$  were  $6 \times 10^{34}$  years, the proton decay signal rate would be almost equivalent to the rate of the background events. Therefore, it will be important to reduce the number of the background events in order to make a clean discovery of proton decay in future experiments. If necessary, the remaining background can be further reduced to improve the signal/background ratio. For example, Fig. 14 suggests that the background rate could be reduced by an order of magnitude by applying a tighter momentum cut ( $P_{tot} < 100$  MeV/c), while the signal efficiency would be reduced only by a factor of 2.3 [11].

With the present SK exposure (0.092 Mtyr), the expected background rate for  $E_\nu < 3$  GeV is  $0.15^{+0.04}_{-0.03}$  (stat)  $^{+0.04}_{-0.05}$  (syst) events. This result is consistent with the observed lack of candidates in the SK experiment [9, 10].

According to Tbl. II, the background rate determination can be improved by reducing uncertainties of the atmospheric neutrino flux, and uncertainties of total and anti-neutrino interaction rates with the atmospheric neutrino flux in future.

Note that the background rate for the  $p \rightarrow \mu^+\pi^0$  mode can be determined in the same way just by replacing the atmospheric  $\nu_e + \bar{\nu}_e$  flux with  $\nu_\mu + \bar{\nu}_\mu$  flux for the CC background and the detection probability of the “ $p \rightarrow e\pi^0$ ” sample with that of the “ $p \rightarrow \mu\pi^0$ ” sample in the proton decay detectors.

### IV. CONCLUSION

The atmospheric neutrino background to searches for  $p \rightarrow e^+\pi^0$  has been experimentally studied using an accelerator neutrino beam and a water Cherenkov detector for the first time. The K2K KT detector, with the same target material and detection technique as SK, accumulated data equivalent to atmospheric neutrino exposures of 15.9 and 4.5 Mtyr for the CC and NC background events, respectively.

Two neutrino interaction simulation programs, NEUT and NUANCE, were evaluated and found to reproduce accelerator neutrino beam interactions in water within the measurement

errors. Both should therefore reliably model the atmospheric neutrino background to  $p \rightarrow e^+\pi^0$  searches.

This is the first determination of the background rate using data for the SK-type water Cherenkov detectors. We measured the rate of neutrino and final-state nuclear interactions of the background events. To measure the background rate from the KT data themselves, almost identical selection criteria as for  $p \rightarrow e^+\pi^0$  searches were applied. A total of 24 “proton decay”-like events were identified. A re-weighting procedure was applied using the atmospheric neutrino flux and detection efficiency (40 %) for the SK proton decay search, and the resulting background rate for  $E_\nu < 3$  GeV (where about 76 % of the background events is expected in SK according to the MC study) is  $1.63^{+0.42}_{-0.33}$  (stat)  $^{+0.45}_{-0.51}$  (syst) Mtyr $^{-1}$ .

This experimentally determined background rate is consistent with no candidates being observed over the 0.1 Mtyr exposure of the SK-I experiment.

This result shows that about two background events per year would be expected in possible future one-megaton-scale detectors. Assuming a finite proton lifetime by an order beyond the present limit, the rate of signal would be similar to the expected background rate, both in these proposed detectors as well as in a still-running Super-Kamiokande. Therefore, further reduction of the background events will be crucial in the future.

### V. ACKNOWLEDGMENTS

We thank the KEK and ICRR directorates for their strong support and encouragement. K2K was made possible by the inventiveness and the diligent efforts of the KEK-PS machine group and beam channel group. We gratefully acknowledge the cooperation of the Kamioka Mining and Smelting Company. This work has been supported by the Ministry of Education, Culture, Sports, Science and Technology of the Government of Japan, the Japan Society for Promotion of Science, the U.S. Department of Energy, the Korea Research Foundation, the Korea Science and Engineering Foundation, NSERC Canada and Canada Foundation for Innovation, the Istituto Nazionale di Fisica Nucleare (Italy), the Ministerio de Educación y Ciencia and Generalitat Valenciana (Spain), the Commissariat à l’Energie Atomique (France), and Polish KBN grants: 1P03B08227 and 1P03B03826.

---

[1] J.C.Pati and A.Salam, Phys.Rev.Lett. 31, 661 (1973).  
[2] H.Georgi and S.L.Glashow, Phys.Rev.Lett. 32, 438 (1974).  
[3] P.Langacker, Phys.Rep. 72, 185 (1981).  
[4] J.Ellis *et al.*, Phys.Lett. B252, 53 (1990); J.Ellis *et al.*, Phys.Lett. B371, 65 (1996).  
[5] N.T.Shaban and W.J.Stirling, Phys.Lett. B291, 281 (1992).  
[6] D.G.Lee, R.N.Mohapatra, M.K.Parida and M.Rani, Phys.Rev. D51, 229, (1995).  
[7] Y.Fukuda *et al.*, Nucl.Instrum.Meth. A501, 418-462 (2003).  
[8] M.Shiozawa *et al.*, Phys. Rev. Lett. 81, 3319-3323 (1998).  
[9] M.Shiozawa, NOON2003 Conf.Proc., 455-460 (2003).

[10] M.Shiozawa, ICRC Conf.Proc., 1633-1636 (2003).  
[11] M.Shiozawa, AIP Conf.Proc. 533, 21-24 (2000).  
[12] M.Koshiba, Phys.Rept. 220, 229-381 (1992).  
[13] C.K.Jung, AIP Conf.Proc. 533, 29-34 (2000).  
[14] K.Nakamura, Front.Phys. 35, 359-363 (2000).  
[15] Y.Suzuki *et al.*, hep-ex/0110005.  
[16] K.Nakamura, Int.J.Mod.Phys. A18, 4053-4063 (2003).  
[17] A. de Bellefon *et al.*, hep-ex/0607026.  
[18] G.Battistoni *et al.*, Nucl. Instr. Meth. A219, 300 (1984).  
[19] M.Derrick *et al.*, Phys. Rev. D30, 1605 (1984).  
[20] W.A.Mann *et al.*, Phys. Rev. D34, 2545 (1986).

- [21] C.Berger *et al.*, Nucl. Instr. Meth. A302, 406 (1991).
- [22] M.H.Ahn *et al.*, Phys.Rev. D74, 072003 (2006).
- [23] T.Ishii *et al.*, Nucl.Instrum.Meth. A482, 244 (2002).
- [24] M.Honda, T.Kajita, K.Kasahara, and S.Midorikawa, Phys.Rev. D70, 043008 (2004), astro-ph/0404457.
- [25] Y.Ashie *et al.*, Phys.Rev. D71, 112005 (2005).
- [26] Y.Hayato, Nucl.Phys.Proc.Suppl. 112, 171 (2002).
- [27] S. Nakayama *et al.*, Phys.Lett. B619, 255-262 (2005).
- [28] KEK Data Acquisition Development Working Group, KEK Report 85-10, 1985; H.Ikeda *et al.*, Nucl.Instrum.Meth. A320, 310 (1992); T.Tanimori *et al.*, IEEE Trans.Nucl.Sci. NS-36, 497 (1989).
- [29] M.Shiozawa, Nucl.Instrum.Meth. A433, 240-246 (1999).
- [30] R.Brun and F.Carminati, CERN Programming Library Long Writeup W5013 (1993).
- [31] H.Gallagher, D.Casper, Y.Hayato, and P.Sala, Nucl. Phys. Proc. Suppl. 139, 278-285 (2005).
- [32] D.Casper, Nucl.Phys.Proc.Suppl. 112, 161 (2002).
- [33] C.Zeitnitz and T.A.Gabriel, Nucl.Instrum.Meth. A349, 106 (1994).
- [34] A.Bodek and U.K.Yang, Nucl.Phys.Proc.Suppl. 112, 70 (2002).